A laboratory experiment for a new free-standing pupil mask coronagraph

K. Haze*[a], K. Enya[a], T. Kotani[a], L. Abe[b], T. Nakagawa[a], H. Matsuhara[a], T. Sato[c], T. Yamamuro[d]

[a] Japan Aerospace Exploration Agency Japan, 3-1-1 Yoshinodai, Chuo-ku, Sagamihara, Kanagawa, Japan 252-5210; [b] Laboratoire Lagrange, UMR 7293 Theory and Observation in Planetology Université de Nice-Sophia Antipolis, CNRS, OCA, Parc Valrose, Nice, France F-06108; [c] Agency of Industrial Science and Technology, 16-1 Onogawa, Tsukuba, Ibaraki, Japan 305-8569; [d] OptCraft, 3-16-8-101 Higashihashimoto, Midori-ku, Sagamihara, Kanagawa, Japan 252-0144

ABSTRACT

This paper presents the results of a laboratory experiment on a new free-standing pupil mask coronagraph for the direct observation of exoplanets. We focused on a binary-shaped pupil coronagraph, which is planned for installation in the next-generation infrared space telescope SPICA. Our laboratory experiments on the coronagraph were implemented inside a vacuum chamber (HOCT) to achieve greater thermal stability and to avoid air turbulence, and a contrast of 1.3×10^{-9} was achieved with PSF subtraction. We also carried out multi-color/broadband experiments to demonstrate that the pupil mask coronagraph works, in principle, at all wavelengths. We had previously manufactured a checker-board mask, a type of binary-shaped pupil mask, on a glass substrate, which had the disadvantages of light loss by transmission, ghosting from residual reflectance and a slightly different refractive index for each wavelength. Therefore, we developed a new free-standing mask in sheet metal, for which no substrate was needed. As a result of a He-Ne laser experiment with the free-standing mask, a contrast of 1.0×10^{-7} was achieved for the raw coronagraphic image. We also conducted rotated mask subtractions and numerical simulations of some errors in the mask shape and WFEs. Speckles are the major limiting factor. The free-standing mask exhibited about the same ability to improve contrast as the substrate mask. Consequently, the results of this study suggest that the binary-shaped pupil mask coronagraph can be applied to coronagraphic observations by SPICA and other telescopes.

Keywords: Coronagraphs, Technology demonstrations, Exoplanets

1. INTRODUCTION

The enormous contrast in flux between the central star and associated planets is the primary difficulty in the direct observation of exoplanets. For example, if the solar system is observed from a distance, the expected contrast between the Sun and the Earth is $\sim 10^{-10}$ in the visible light region and $\sim 10^{-6}$ in the mid-infrared region (Traub & Jucks 2002). Therefore, the development of stellar coronagraphs, which can improve the contrast between the star and the planet, is needed. Of the various kinds of coronagraph (e.g., Guyon et al. 2006, see their Table1), we have focused on a binary-shaped pupil mask coronagraph (Jacquinot & Roizen-Dossier, 1964; Spergel, 2001; Vanderbei et al., 2003a,b, 2004; Kasdin et al., 2003, 2005a,b; Green et al., 2004; Tanaka et al., 2006; Enya & Abe, 2010; Enya et al., 2011). The reasons for using this coronagraph are that it is robust against pointing errors, it can, in principal, be used to make observations over a wide wavelength range and it is relatively simple. Also, the adoption of a binary-shaped pupil mask coronagraph for SPICA is being considered (Enya et al., 2010). We are currently promoting the development of the coronagraph to make it fit for practical use.

*haze@ir.isas.jaxa.jp

1.1 Our previous experiments

In previous experiments we have used a checkerboard pupil mask, which is a type of binary-shaped pupil mask, which can reduce the amount of diffracted light from the central star, known as "the dark region". A checkerboard mask ("Mask 2"), comprising a patterned 100nm thick aluminum film on a BK7 glass substrate, was manufactured using nano-fabrication techniques with electron beam lithography. The theoretical contrast, inner working angle (IWA), and outer working angle (OWA) were 10^{-7}, $3\lambda/D$, and $30\lambda/D$, respectively, where λ is wavelength and D is the diagonal of the mask.

The high contrast performance (1.1×10^{-7}) of the binary-shaped pupil mask coronagraph was confirmed (Enya et al. 2007). Further development and verification were required for this coronagraph to be installed on a telescope. In space telescopes, the WFE caused by imperfections in the optics is an important limiting factor in the contrast of a coronagraph. For an actual observation, it is necessary to make observations over a wide wavelength band, and it would be beneficial to make observations using multiple bands.

Therefore we conducted a number of multi-color/broadband coronagraph experiments in a vacuum chamber using a binary-shaped pupil mask, which in principle should work at all wavelengths. The aim of this work is to demonstrate that subtraction of the Point Spread Function (PSF) and multi-color/broadband experiments using a binary-shaped pupil mask coronagraph would help improve the contrast in observations of exoplanets. Mask 2 was used. We improved the temperature stability by installing the coronagraph optics in HOCT (High-dynamical range Optical Coronagraph Test bed). HOCT is a test bed which has a vacuum chamber while controlling the temperature of the optical bench, and covering the vacuum chamber with thermal insulation layers, as shown in Figure 1. Active wavefront control was not applied in this work. We evaluated how much the PSF subtraction contributed to the high-contrast observation by subtracting images obtained through the coronagraph. We also carried out multi-color/broadband experiments in order to demonstrate more realistic observations using Super luminescent Light Emitting Diodes (SLEDs) with center wavelengths of 650 nm, 750 nm, 800 nm, and 850 nm. A contrast of 2.3×10^{-7} was obtained for the raw coronagraphic image and a contrast of 1.3×10^{-9} was achieved after PSF subtraction with a He-Ne laser with a wavelength of 632.8nm (Haze et al., 2009, 2011). Thus, the contrast was improved by around two orders of magnitude from the raw contrast by subtracting the PSF. We achieved contrasts of 3.1×10^{-7}, 1.1×10^{-6}, 1.6×10^{-6}, and 2.5×10^{-6} for bands at 650 nm, 750 nm, 800 nm, and 850 nm, respectively, in multi-color/broadband experiments (Haze et al., 2011). The results showed that the contrast within each of the wavebands was significantly improved compared with the non-coronagraphic optics. We demonstrated that PSF subtraction is potentially beneficial for improving the contrast of a binary-shaped pupil mask coronagraph; significant improvements in contrast were achieved with multi-color/broadband light sources.
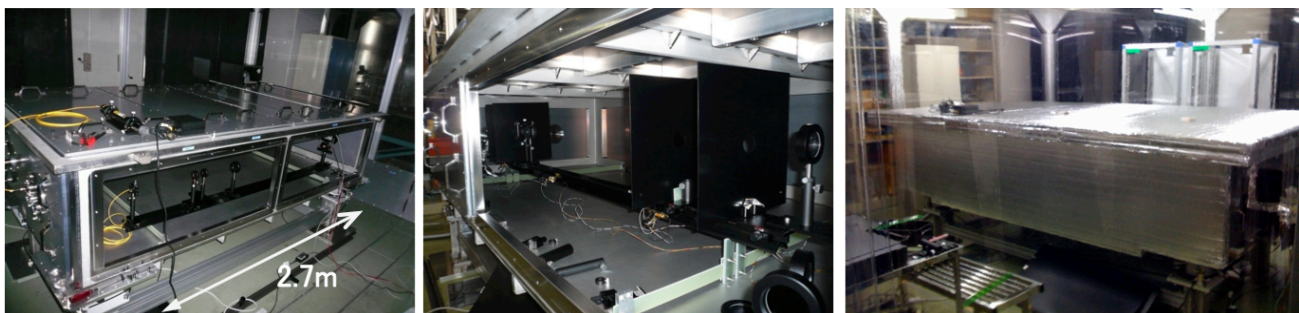

Figure 1. High-dynamicrange Optical Coronagraph Testbed (HOCT). Right panel shows HOCT covered by thermal insulation.

2. EXPERIMENTS

In the work described in the previous section, we demonstrated the basic properties of binary-shaped pupil mask coronagraphs. However, the glass substrate for the mask, which has been successfully used in previous experiments with visible light, has the following disadvantages; it suffers from transmission losses, ghosting from residual reflectance occurs, and the refractive index is wavelength dependent.

On the other hand, a free-standing mask has the advantages of no transmission losses, no ghosting from residual reflectance and a refractive index that is independent of wavelength. Therefore, we developed a new free-standing mask made from sheet metal that requires no substrate (Enya et al., 2012). We conducted free-standing mask coronagraph experiments and evaluated the contrast performance of the free-standing mask. Details are discussed in the following section.

2.1 New free-standing pupil mask

In this section, we describe the design and performance of the new free-standing mask (Figure 2). The mask is a checkerboard mask (Figure 3(a)). There are four dark regions near to the core of the PSF, as shown in Figure 3 (b). The designed contrast, IWA, and OWA are 10^{-10}, $5.4\lambda/D$, and $50\lambda/D$, respectively. The mask, formed of copper laminate, was fabricated by high-accuracy electroforming. We increased the pupil-mask size from 2mm to 10mm because of the difficulty in making small free-standing masks. A photomask with the pattern was made first, and then the free-standing mask was made by photolithography using the photomask. The manufacturing processes of the photomask and the free-standing mask are described in Enya et al., (2012).

2.2 Optical system

The optical system is shown in Figure 4. The light source is a He-Ne laser. The distinctive configuration of this experiment is as follows. We used a free-standing mask, 10mm in size, designed to give a contrast of 10^{-10}. The mask is larger than Mask 2, which is 2mm in size. A CCD camera was set up in the chamber. We used $3.4\times$ relay optics after the focal plane mask with the change of mask size and camera position.

2.3 Imaging procedure

To obtain a high-contrast image, we measured the core and the dark region separately, since each have different exposure times.

The core images of the coronagraphic PSF were taken with a combination of several sets of exposure times (0.3, 3, 10s) using two ND filters. After each imaging process, the laser source was turned off and a "dark frame" measurement was taken with the same exposure time and the same ND filters. The dark frame was subtracted from the image with the laser light on and we obtained a "raw" coronagraphic image (Figure 5(a)).

The dark region of the coronagraphic image was observed with 300s exposure using a square hole focal-plane mask. We took four images (DR1 - DR4) shifting the focal-plane mask, where DR1 - DR4 are the dark regions corresponding to the quadrants around the core, shown in Figure 3(b). A "dark frame" was taken with 300s exposure and this was then subtracted from the dark region image with the laser light on. The observed dark regions of the raw coronagraphic image are shown in Figure 5(b)(c)(d)(e).
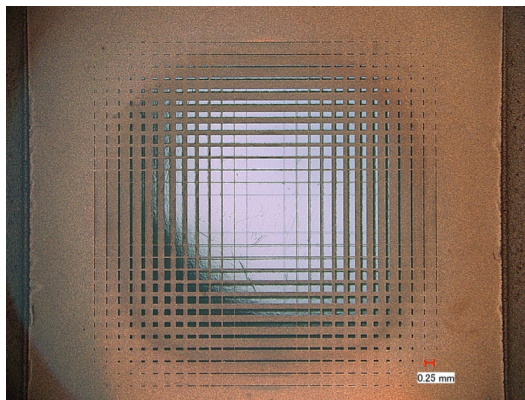

Figure 2. The new free-standing mask formed of copper laminate. The transmissive region is 10mm on a side.
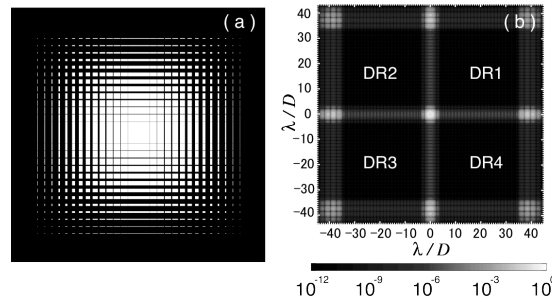
Figure 3. Panel (a) Design of the free-standing mask. The transmissivities of the black and white regions are 0 and 1, respectively. Panel (b) Simulated coronagraphic PSF, using the mask design shown in panel (a).
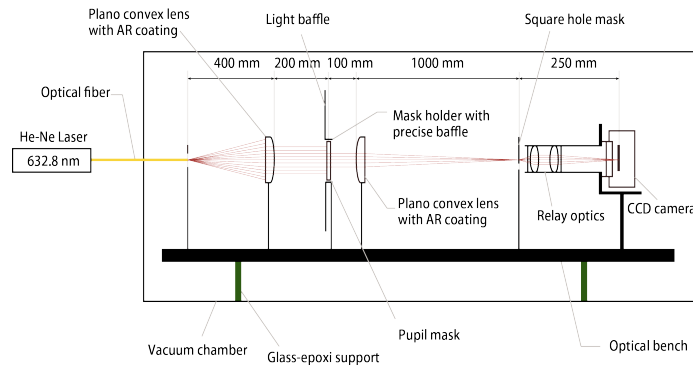

Figure 4. The configuration of the optical system.

3. RESULT AND DISCUSSION

3.1 Contrast of the free-standing mask

The observed coronagraphic images are shown in Figure 5. Figure 6 shows diagonal profiles of the observed coronagraphic PSF, the designed coronagraphic PSF and the Airy PSF. The images and profiles of the core of the observed coronagraphic PSF are quite consistent with those expected from theory. The relative intensity over most of the area of the dark region was less than 10^{-6}, as shown in Figure 6. We evaluated the contrast between the areal mean of the observed dark region and the peak of the core. The contrast values are 9.6×10^{-8}, 9.6×10^{-8}, 9.5×10^{-8} and 1.2×10^{-7} for DR1, DR 2, DR 3 and DR4, respectively. The average contrast for all the dark regions is $1.0\text{x}10^{-7}$. Figure 5(b)(c)(d)(e) also exhibits irregular speckles in the dark regions, which are not predicted by the theoretical PSF of the mask.

It was demonstrated that the free-standing mask has the capacity to improve the contrast to 1.0×10^{-7}, which was achieved for the raw coronagraphic image by areal averaging of all the observed dark regions. Because a free-standing masks is independent of wavelength it can be use in the infrared region. For instance, it can also be installed in the next-generation infrared telescope SPICA. Nevertheless the mask pattern needs to be changed from a checker-board design to a new mask pattern that takes into consideration the pupil shape of the telescope with the secondary mirror and spiders (Enya & Abe, 2010).

3.2 Rotated mask subtraction

The results of the free-standing mask experiments demonstrated that the contrast was 1.0×10^{-7}, while the designed contrast is 10^{-10}. Speckles are the major limiting factor. We suppose that the major factors causing speckles are (1) errors in the pupil-mask shape and (2) other errors in the optical-system apart from the mask.

We consider that rotating the pupil-mask only would separate errors in the mask shape from the other errors, because we expect that speckles from errors in the mask shape rotate with the mask.

First, we subtracted the images without mask rotation to confirm the stability of the optical system. We evaluated the contrast between the standard deviation of the subtracted dark region and the peak of the core. As a result, a contrast of 8.1×10^{-8} was obtained. The result shows that the contrast was significantly improving compared with the raw contrast. Therefore, it is worth evaluating the improvement attained by rotated mask subtraction. So, we rotated the mask 90 degrees around the central axis perpendicular to the mask surface to confirm whether the intensity distribution of the irregular speckle pattern changed. We subtracted the image after mask rotation (Figure 7) from the image before mask rotation (Figure 5). Rotated mask subtraction can be done in two different ways (Rotated mask subtraction 1 and 2).

1. Rotated mask subtraction 1 is where the image is rotated -90 degrees after mask rotation and subtracted from the image before mask rotation. In other words, this is a way of subtracting speckles in the dark regions associated with the direction of the mask. If the speckles are only due to errors in the mask shape, rotated mask subtraction1 is expected to improve the contrast. This is because speckles in the dark regions are associated with the direction of the mask in this case. We rotated the images -90 degrees after mask rotation. We shifted the core image before mask rotation to fit the center of the core before and after mask rotation, and then the shift was applied to the dark region images. We increased the intensity of the dark region before mask rotation by 1.27 times to be consistent with both the areal mean of the dark regions before and after mask rotation. We subtracted the images after adjusting the position of the PSF and the intensity as above. There are four ways to carry out the subtraction (DR1-DR1', DR2-DR2', DR3-DR3', DR4-DR4'). Figure 8 shows the PSF after rotated mask subtraction 1. Comparing the speckle patterns before and after mask rotation, the speckle patterns are completely different, as shown in Figure 5 and Figure 7. Also, the residuals on the rotated mask subtraction image, as shown in Figure 8, are different from the residuals from misalignment of the images. Therefore, the residuals from misalignment of the images are not the main component of the residuals in the subtracted image. We evaluated the contrast between the standard deviation of the dark region after rotated mask subtraction 1 and the peak of the core. The approach used to estimate the contrast using the standard deviation of the dark region was as adopted in Biller et al. (2009). As a result, contrasts of 1.3×10^{-7}, 1.4×10^{-7}, 1.3×10^{-7} and 1.5×10^{-7} for DR1 - DR1', DR2 - DR2', DR3 - DR3' and DR4 - DR4', respectively, were achieved for the images from rotated mask subtraction 1. The contrasts showed no improvement compared with the contrasts before subtraction. In other words, this means the speckles are not due to errors in the mask shape only, but are also due to errors in the optical-system. We consider that the errors in the optical-system consist of WFEs, non-uniform intensity, stray light and so on.

2. Rotated mask subtraction 2 is where the image after mask rotation is subtracted from the image before mask rotation. If the mask shape and repeatability of the mask position are perfect, rotated mask subtraction 2 is expected to improve the contrast. This is because the errors in the optical-system, such as WFEs are common to images both before and after mask rotation. We shifted the core image before mask rotation to fit the centers of the core before and after mask rotation, and then this shift was applied to the dark region images. We increased the intensity of the dark region before mask rotation by 1.27 times to be consistent with both the areal mean of the dark regions before and after mask rotation. We subtracted the images after adjusting the position of the PSF and the intensity as above. There are four ways to carry out the subtraction (DR1-DR2', DR2-DR3', DR3-DR4', DR4-DR1'). Figure 9 shows the PSF after rotated mask subtraction 2. We evaluated the contrast between the standard deviation of the dark region after rotated mask subtraction 2 and the peak of the core. As a result, contrasts of 1.2×10^{-7}, 1.7×10^{-7}, 1.7×10^{-7}, 1.4×10^{-7} for DR1 - DR2', DR2 - DR3', DR3 - DR4', DR4 - DR1', respectively, were achieved for the images from rotated mask subtraction 2. No improvement in the contrasts was found compared with the contrasts before subtraction. These results show the mask shape and/or the repeatability of the mask position are not perfect.

These rotated mask subtraction results show that speckle is not just due to errors in the mask shape, but arise because of errors in the optical-system also. The speckles are due to errors in the optical-system (e.g., the WFE, non-uniform intensity and stray light) or the combined effect of errors in the mask shape and errors in the optical-system apart from the mask. A useful way of distinguishing between errors in the mask shape, errors in the optical-system and the error in replicating the mask position is to simulate the effects of these errors.
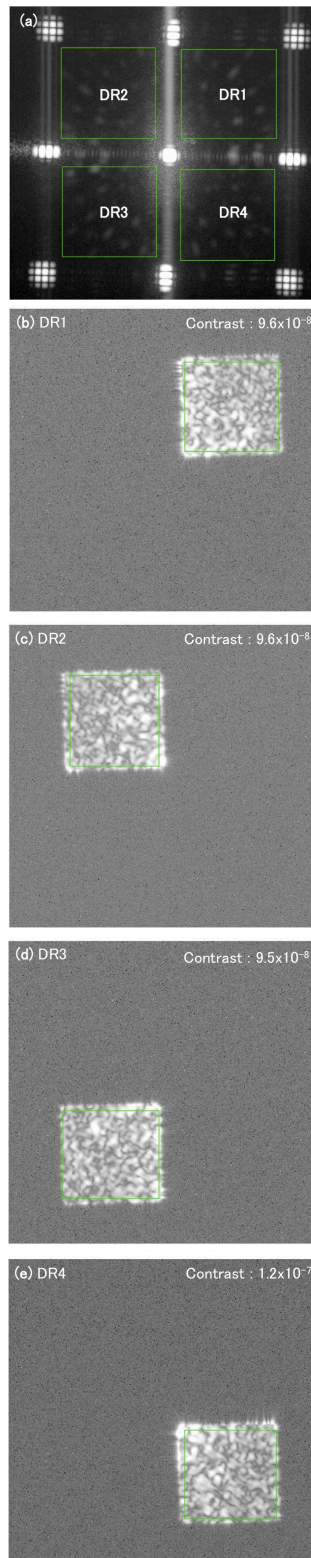
Figure 5. Observed coronagraphic images before mask rotation. Panel (a): an image including the core of the PSF. Panels (b), (c), (d) and (e): raw images of the dark regions. The areal means in each green rectangle in DR1 - 4 were obtained.
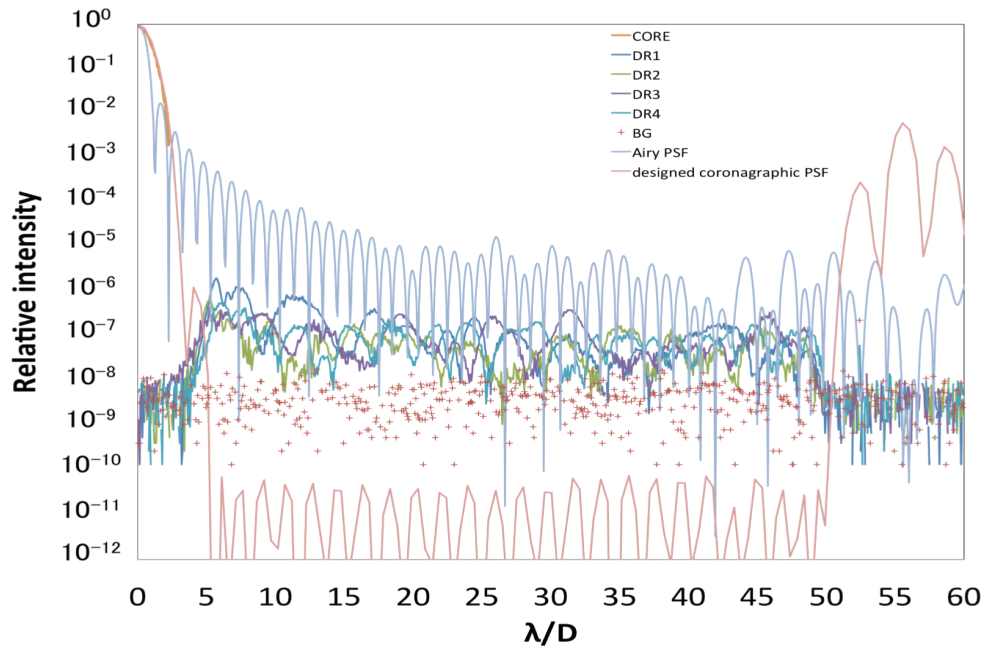
Figure 6. Diagonal profiles of the observed coronagraphic PSF, designed coronagraphic PSF and Airy PSF. Each profile is normalized by the peak intensity.

3.3 Numerical simulations of some mask shape errors

We simulated the PSFs with only errors in the mask shape. We considered a simplified case of an across-the-board increase in the line width of the mask pattern which blocks the light. Figure 10 shows simulated PSFs from across-the-board 5, 10, 15, 20μm increases in the line width of the free-standing mask. In the case of an across-the-board 20μm increase in line width, the smallest holes, where light passes through the mask, are closed. When we checked the holes of the free-standing mask using a digital microscope (VHX-900, KEYENCE), we found holes in the positions expected from the mask design. Thus, the case of an across-the-board 20μm increase is worse than achieved in reality and is an extreme case. So, we ignored the case of an across-the-board increase of more than 20μm. Even in the case of an across-the-board 20μm increase in line width, the contrast in the dark region was not worse than 10^{-7}. Therefore, this suggests that the speckle was not only due to errors in the mask shape. This result of the numerical simulations of the mask shape errors is consistent with the result of Rotated mask subtraction 1.

3.4 Numerical simulations of WFEs

In this section, we show the results of simulations of the PSFs without errors in the mask shape, but with only wavefront errors. First of all, we simulated the PSF that reproduces the experimental raw contrast ($\sim 10^{-7}$) by using the appropriate wavefront error. One of the preferred metrics used for specifying wavefront errors is the power spectral density (PSD). This is computed from the amplitudes of the spatial frequency components present in the Fourier spectrum of the surface height of the pupil-plane. With reference to Sidick (2009), we used the following Lorentzian equation as our PSD function:

$$PSD = \frac{\sigma_0^2 A}{h_0} \frac{1}{1 + (\rho_{mn}/\rho_{HP})^p},$$

(1)

where σ_0 is the rms value, A is the mask size, ρ_{mn} is the spatial frequency (m^{-1}), ρ_{HP} is the half-power frequency (m^{-1}), p is a power law, and $h0 = \sum_{m=1}^{M} \sum_{n=1}^{N} \frac{1}{1 + (\rho_{mn}/\rho_{HP})^p}$.

We chose ρ_{HP} = 4.3 m^{-1} with reference to the HST mirror (Borde & Traub, 2006). Substituting particular values for σ_0 and p, we simulated the PSFs. We chose the best fit which minimizes the sum of the squared residuals, a residual being the difference between the observed and simulated radial averages, as shown in Figure 11. In this simulation, the RMS from the wavefront error is 3.5 nm ($\lambda_0/180$), where λ_0 = 632.8 nm.

Second, we discuss the results of Rotated mask subtraction 2 using the result from the WFE simulation. Specifically, we simulated the PSFs from the error in replicating the mask position. We estimated an upper limit for the error due to the mask position. There are two reasons for the error in mask position to occur when the mask is rotated.

1. An error in the position of the mask holder.
   The mask holder has 4 threaded holes for inserting rods on the left, right, top and bottom. The mask holder, including the position of the threaded holes, has good central symmetry and a high accuracy (< 0.1mm). The error might include a tilt error (<1°) because of the threaded anchorage. The contribution of the tilt error to the positional error of the mask holder is negligibly-small.
2. The error in position between the mask and the mask holder.
   The mask holder has a mask location allowance. The mask holder is about 1mm larger than the mask in height and width.

Therefore, we assumed the upper limit of the error in replicating the mask position is 1mm and simulated the PSF from the mask position shifted 1mm on the pupil-plane as shown in Figure 12. We subtracted the PSF after shifting from that before shifting the mask. Figure 12(e) shows the PSF after subtraction. We evaluated the contrast between the standard deviation of the dark region and the peak of the core. As a result, a contrast of 6.4×10^{-8} was obtained. The contrast of 6.4×10^{-8} was not as bad as the contrast (1.2×10^{-7}) after rotated mask subtraction 2. Furthermore, the result (6.4×10^{-8}) was not as bad as the contrast (8.1×10^{-8}) without mask rotation confirming the stability of the optical system. We can see from the above that the error in replicating the mask position is not the main factor after rotated mask subtraction 2.

It is suggested from the above that one of the main factors of the results after rotated mask subtraction 2 is the low stability of the optical system. A qualitative explanation for the result of rotated mask subtraction 2 giving a poorer contrast of 1.2×10^{-7} than the contrast of 8.1×10^{-8} without mask rotation is that a longer time interval between observations is required for rotated mask subtraction 2 than subtraction without mask rotation.

4. SUMMARY AND CONCLUSION

This paper presents a new free-standing pupil mask coronagraph for practical use which provides superior performance in improving contrast. We focused on a binary-shaped pupil coronagraph, which is planned for installation in the next-generation infrared space telescope SPICA. From the results of our laboratory experiments on the coronagraph, which were carried out inside a vacuum chamber to achieve higher thermal stability and to avoid air turbulence, a contrast of 1.3×10^{-9} was achieved for PSF subtraction. We also carried out multi-color/broadband experiments with center wavelengths of 650nm, 750nm, 800nm and 850nm to demonstrate that the pupil mask coronagraph works, in principle, at all wavelengths. A checker-board mask on a glass substrate has the disadvantages of transmission losses, ghosting from residual reflectances and a slightly different refractive index for each wavelength. Therefore, we developed a new free-standing sheet metal mask without the need for a substrate. The free-standing mask can be used for infrared observations which have a great advantage over visible light observations in that the contrast between the star and the planet is much less. In an experiment with a He-Ne laser and the free-standing mask, we achieved contrasts of 9.6×10^{-8}, 9.6×10^{-8}, 9.5×10^{-8} and 1.2×10^{-7} in DR1, DR2, DR3 and DR4, respectively. We also conducted rotated mask subtractions and numerical simulations of errors in the mask shape and WFEs. Speckles are the major limiting factor. A similar significant improvement in contrast was demonstrated with the free-standing mask as with the substrate mask. Consequently, the results of this study suggest that the binary-shaped pupil mask coronagraph can be applied to coronagraphic observations by SPICA and other telescopes.

REFERENCES

[1] Traub, W. A., & Jucks, K. W., "A Possible Aeronomy of Extrasolar Terrestrial Planets," Astro-ph/0205369, (2002).

[2] Guyon, O., Pluzhnik, E. A., Kuchner, M. J., Collins, B., & Ridgway, S. T., "Theoretical Limits on Extrasolar Terrestrial Planet Detection with Coronagraphs," ApJ, 167, 81 (2006).

[3] Jacquinot, P., & Roizen-Dossier, B., "Apodization," Prog. Opt., 3, 29 (1964).

[4] Spergel, D. N., "A New Pupil for Detecting Extrasolar Planets," Astro-ph/0101142 (2001)

[5] Vanderbei, R. J., Spergel, D. N., & Kasdin, N. J., "Spiderweb masks for high-contrast imaging," ApJ, 590, 593 (2003a)

[6] Vanderbei, R. J., Spergel, D. N., & Kasdin, N. J., "Circularly Symmetric Apodization via Star-shaped Masks," ApJ, 599, 686 (2003b)

[7] Vanderbei, R. J., Kasdin, N. J., & Spergel, D. N., "Checkerboard-Mask Coronagraphs for High-Contrast Imaging," ApJ, 615, 555 (2004)

[8] Kasdin, N. J., Vanderbei, R. J., Spergel, D. N., & Littman, M. G., "Extrasolar Planet Finding via Optimal Apodized-Pupil and Shaped-Pupil Coronagraphs," ApJ, 582, 1147 (2003)

[9] Kasdin, N. J., Belikov, R., Beall, J., Vanderbei, R. J., et al., "Shaped pupil coronagraphs for planet finding: optimization, manufacturing, and experimental results," Proc. SPIE, 5905, 128 (2005a)

[10] Kasdin, N. J., Vanderbei, R. J., Littman, M. G., & Spergel, D. N., "Optimal one-dimensional apodizations and shaped pupils for planet finding coronagraphy," Appl. Opt., 44, 1117 (2005b)

[11] Green, J. J., Shaklan, S. B., Vanderbei, R. J., & Kasdin, N. J., "The sensitivity of shaped pupil coronagraphs to optical aberrations," Proc. SPIE, 5487, 1358 (2004)

[12] Tanaka, S., Enya, K., Abe, L., Nakagawa, T., & Kataza, H., "Binary-Shaped Pupil Coronagraphs for High-Contrast Imaging Using a Space Telescope with Central Obstructions," PASJ, 58, 627 (2006)

[13] Enya, K., & Abe, L., "A Binary Shaped Mask Coronagraph for a Segmented Pupil," PASJ, 62, 1407 (2010)

[14] Enya, K., Abe, L., Takeuchi, S., Kotani, T., & Yamamuro, T., "A high dynamic-range instrument for SPICA for coronagraphic observation of exoplanets and monitoring of transiting exoplanets," Proc. SPIE, 8146, 282 (2011)

[15] Enya, K., Tanaka, S., Abe, L., & Nakagawa, T., "Laboratory experiment of checkerboard pupil mask coronagraph," A&A, 461, 783 (2007)

[16] Haze, K., Enya, K., Abe, L., et al., "An AO-free coronagraph experiment in vacuum with a binary-shaped pupil mask," ASR, 43, 181 (2009)

[17] Haze, K., Enya, K., Abe, L., et al., "Multi-Color Coronagraph Experiment in a Vacuum Testbed with a Binary Shaped Pupil Mask," PASJ, 63, 873 (2011)

[18] Enya, K., Haze, K., Kotani, T., & Abe, L., "Comparative study of manufacturing techniques for coronagraphic binary pupil masks: masks on substrates and free-standing masks," PASJ, in press (2012)

[19] Sidick, E., "Power spectral density specification and analysis of large optical surfaces," Proc. of SPIE, 7390, (2009)

[20] Borde, P., & Traub, W. A., "High-Contrast Imaging from Space: Speckle Nulling in a Low-Aberration Regime," ApJ, 638, 488, (2006)
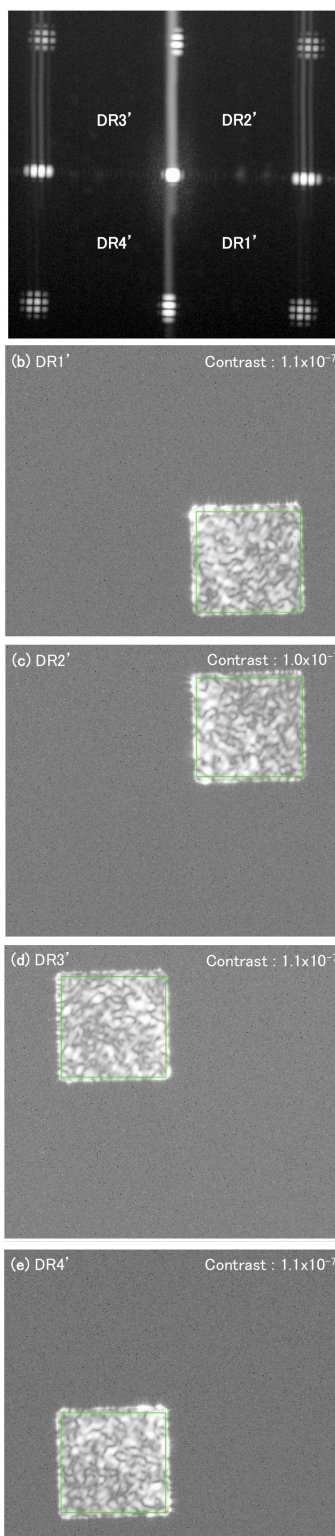
Figure 7. Observed coronagraphic images after mask rotation. Panel (a): an image including the core of the PSF. Panels (b), (c), (d) and (e): raw images of the dark regions. The areal means of each green rectangle in DR1' - 4'were obtained.
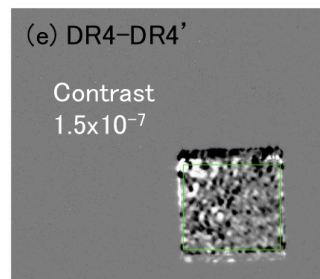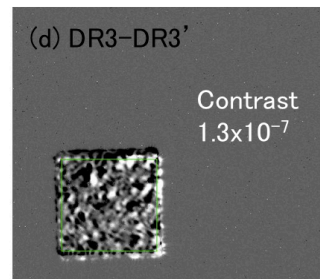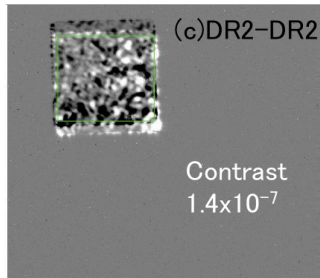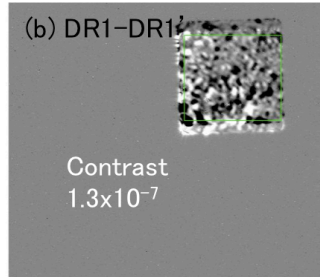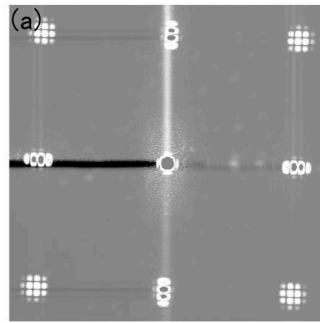
Figure 8. Rotated mask subtraction 1: the way in which the image was rotated by -90 degrees after mask rotation and subtracted from the image before mask rotation. Panel (a): shifting the core image before mask rotation to fit the centers of the cores before and after mask rotation. Panels (b), (c), (d) and (e): images of the results of rotated mask subtraction 1 (DR1-DR1', DR2-DR2', DR3-DR3', DR4-DR4').
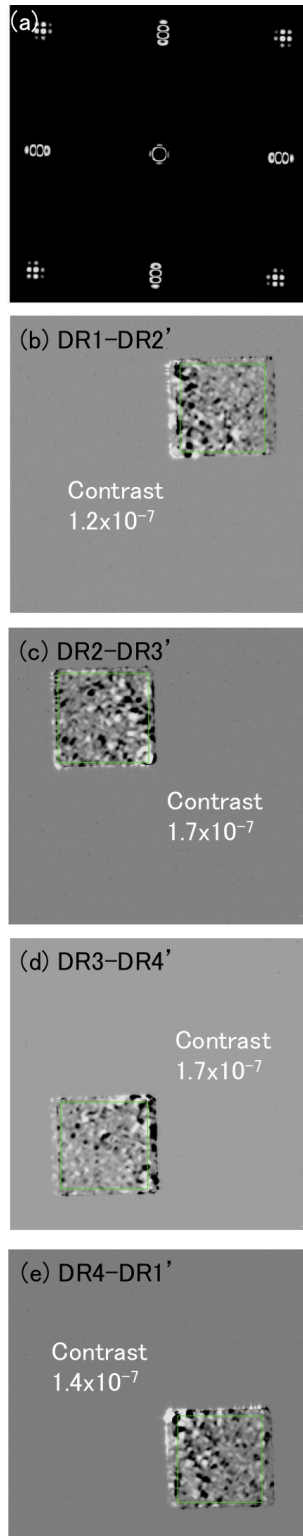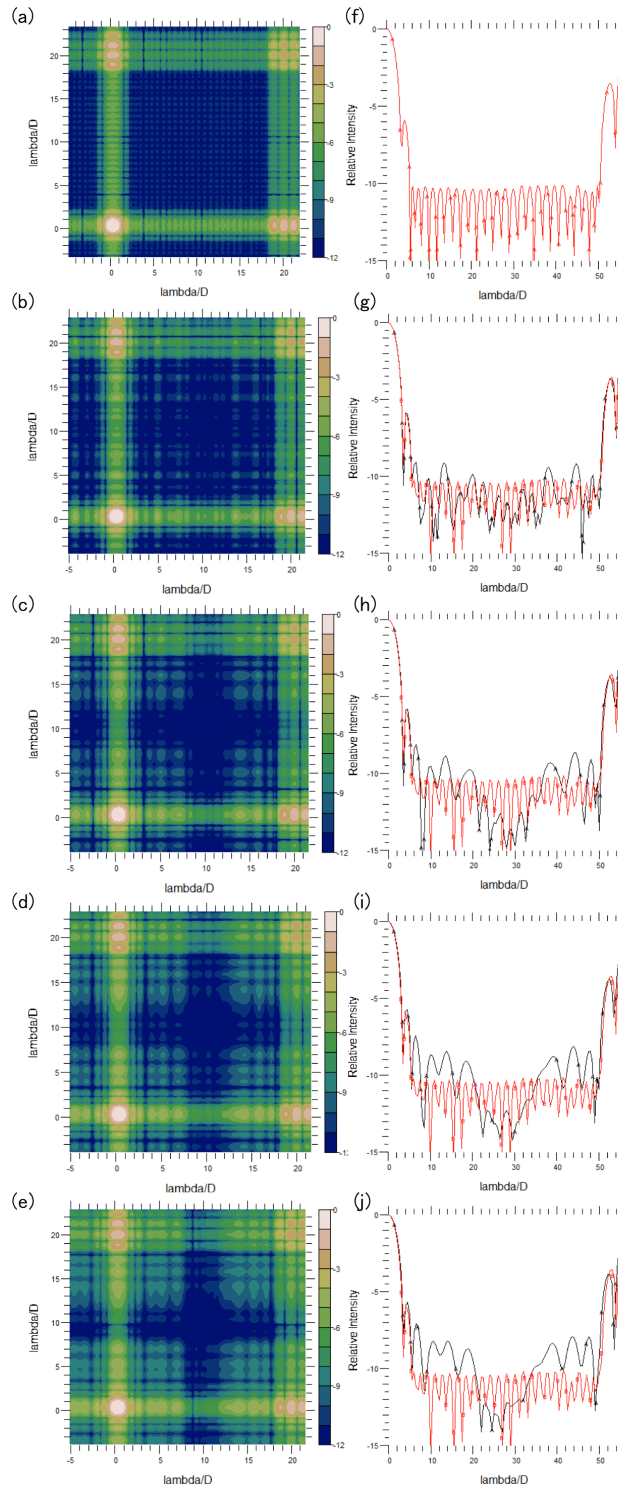
Figure 9. Rotated mask subtraction 2: the way in which the image after mask rotation was subtracted from that before mask rotation. Panel (a): shifting the core image before mask rotation to fit the centers of the cores before and after mask rotation. Panel (b), (c), (d) and (e): images of the results of rotated mask subtraction 2 (DR1-DR2', DR2-DR3', DR3-DR4', DR4-DR1').

Figure 10. Simulated PSFs of the free-standing mask. (a) and (f): Simulated PSFs from the perfect mask. (b) and (g): Simulated PSFs from an across-the- board 5μm increase in the line width of the mask. (c) and (h): Simulated PSFs from an across-the-board10μm increase in the line width of the mask. (d) and (i): Simulated PSFs from an across-the-board 15μm increase in the line width of the mask. (e) and (j): Simulated PSFs from an across-the-board 20μm increase in the line width of the mask. (a), (b), (c), (d) and (e) are simulated images and (f), (g), (h), (i) and (j) are simulated profiles. The red and black lines show the PSFs for the perfect and imperfect masks, respectively. The scale is logarithmic.
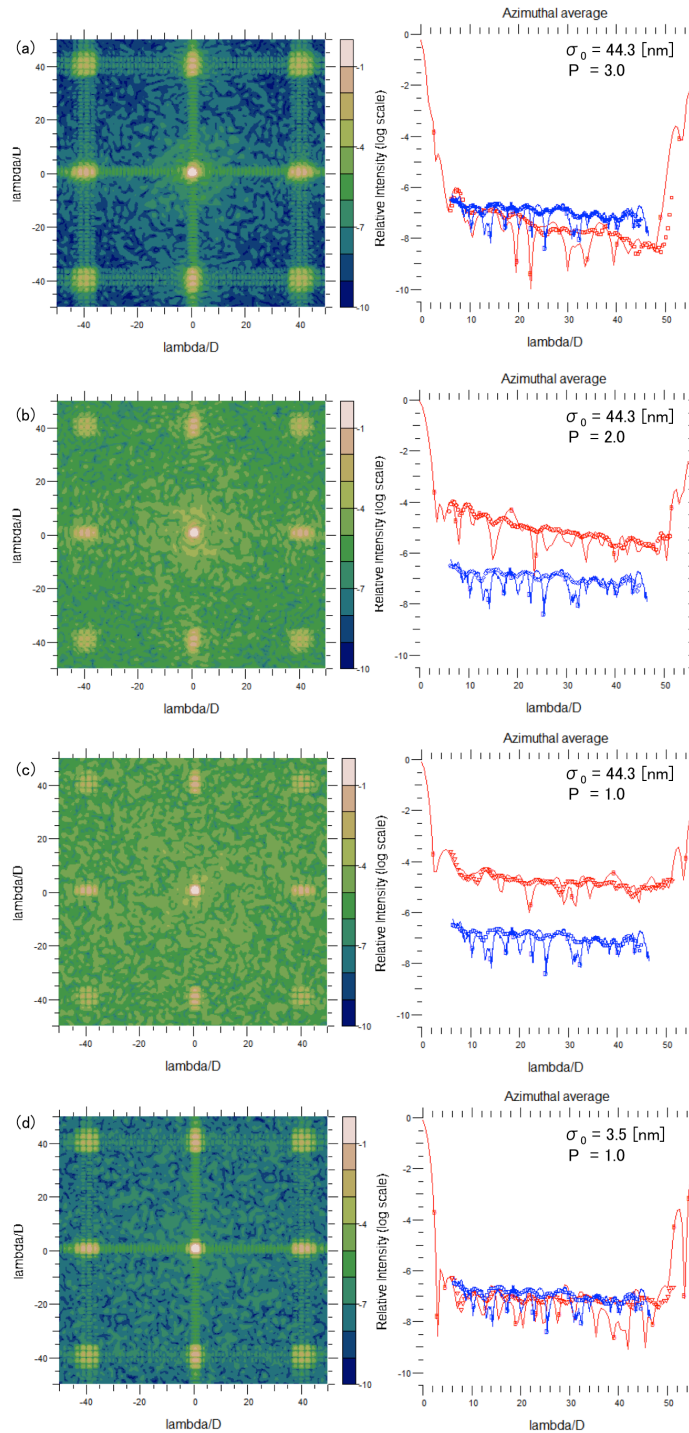
Figure 11. Simulated PSFs of the free-standing mask. Left: Simulated PSFs from the PSDs. Right: Diagonal profiles and average azimuthals of the PSFs. The red line shows the PSF profile and the red triangles show the average azimuthals from the simulation. The blue line shows the PSF profile and the blue squares show the average azimuthals from the experiment. (a)σ_0=44.3 nm (λ0/14)as the SPICA mirror RMS and p=3.0 as a typical telescope mirror (for example, the HST and the VLT mirror have p=2.9 and p=3.1). The error sum of the squares is 1.6×10^{-12}. (b) Changing p=3.0 to p=2.0. The error sum of the squares is 7.9×10^{-8}. (c) Changing p=2.0 to p=1.0. The slope of the simulation was fit to the slope of the experiment. The error sum of the squares is 1.6×10^{-7}. (d) Changing σ_0=44.3 nm to σ_0=3.5nm. This is the best fit for the experimental PSF. The error sum of the squares is as small as 4.4×10^{-13}.
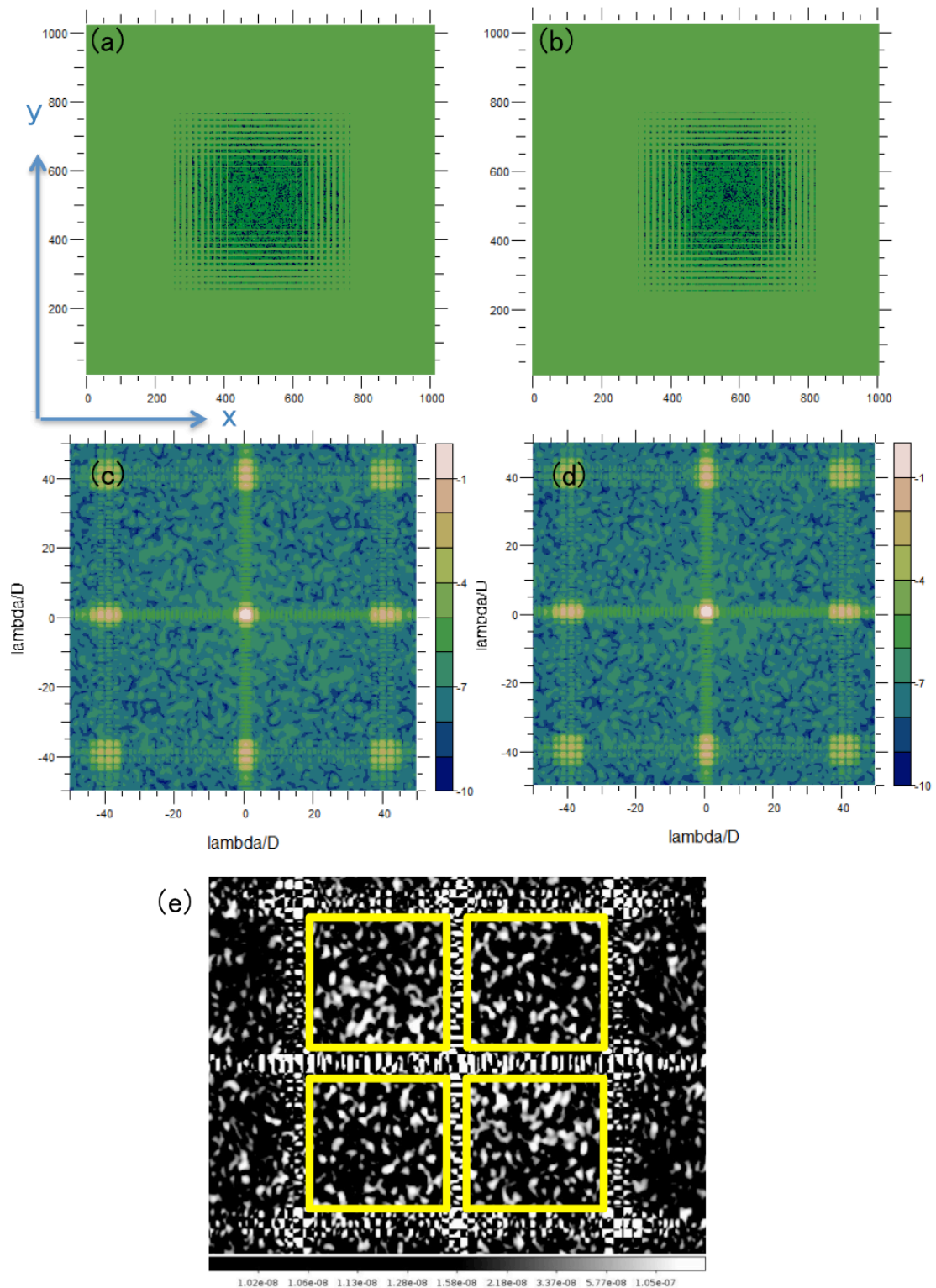
Figure 12. Simulated pupil-plane and PSFs. (a): Simulated surface rough- ness with the binary-shaped pupil mask. (b): Simulated surface roughness with the binary-shaped pupil mask shifted by 1mm in the x-direction. (c): Simulated PSF from (a). (d): Simulated PSF from (b). (e): Image after subtracting (d) from (c). The contrast in the four quadrants (yellow squares) is 6.4×10^{-8}, 6.4×10^{-8}, 6.3×10^{-8}, and 6.4×10^{-8} respectively.